



Ni grade distribution in laterite characterized from geostatistics, topography and the paleo-groundwater system in Sorowako, Indonesia



Asran Ilyas^{a,*}, Koki Kashiwaya^b, Katsuaki Koike^b

^a Mining Engineering Study Program, Geological Engineering Department, Engineering Faculty, Hasanuddin University, Tamalanrea, Makassar 90245, South Sulawesi, Indonesia

^b Department of Urban Management, Graduate School of Engineering, Kyoto University, Katsura C1-2-215, Kyoto 615-8540, Japan

ARTICLE INFO

Article history:

Received 14 May 2015

Revised 13 February 2016

Accepted 1 March 2016

Available online 15 March 2016

Keywords:

Nickel laterite

Ordinary kriging

Topographic control

Groundwater interaction

Saprolite

Goethite

ABSTRACT

Many nickel (Ni) resources and reserves originate from laterite-type deposits in which the grade distributions are generally controlled by the Ni content of the original strata, the degree of weathering, groundwater–rock interaction and the overall strata thickness and distribution. This study aims to clarify the three-dimensional (3D) Ni grade distribution and variation at a mine in the Sorowako area, central Sulawesi Island, Indonesia. Using geostatistics, the relationship between Ni and other chemical components is investigated, as well as topographic effects. Modeling of the grade distribution is achieved using ordinary kriging for single variables because the correlation of Ni with other components is weak. The modeling suggests that relatively high-grade zones are concentrated below a specific topographical type; that is a slight to moderate slope in the 5–19° range. The topography has likely controlled groundwater infiltration through rock fractures formed by the long-term tectonic processes affecting the area and the resultant groundwater interaction with the Ni-bearing strata. The initial Ni is carried as a dissolved phase and precipitated elsewhere, generating the Ni accumulation. By regarding the paleo-groundwater system as one controlling factor on the grade distribution, the thicknesses of limonite and saprolite layers formed by weathering are modeled around rock sampling points with flow being directed from the thinnest to the thickest points in each layer. This model is supported by the presence of Ni-bearing goethite in almost all the samples obtained from the limonite and saprolite layers. Notably, the 3D grade model indicates that the estimated paleo-groundwater flow direction corresponds with the transition from low to high Ni grades around the sampling sites. Weathering is therefore considered to have progressed along the paleo-groundwater flow direction, enhancing the thicknesses of limonite and saprolite layers, as well as the Ni grades, by prolonging the reaction between ferrous minerals and groundwater. The topographic control is considered to have enhanced recharge, infiltration, and reaction of groundwater.

© 2016 Elsevier B.V. All rights reserved.

1. Introduction

Ni deposits occur in two main types: laterite and magmatic sulfide deposits. Laterite deposits are more important in terms of the production volumes of Ni, with 70% of the global Ni demand originating from such (Dalvi et al., 2004). Although Ni laterite deposits are understood to have been generated by intense weathering of ultramafic igneous rocks, the Ni grade distribution is typically highly complicated by many interacting factors. These factors include the parent rock type, meteorological conditions, topography, tectonic setting, geological structure, groundwater, composition of organic material, and rates of weathering (Brand et al., 1998; Gleeson et al., 2003). One or more of these factors may be the predominant factor controlling the Ni grade distribution; however, they may vary between deposits and even

within the same deposit. This causes the Ni grade distribution to be highly changeable and unpredictable.

Many studies have been devoted to understanding the enrichment processes of Ni in laterite deposits, taking the host rock and mineral composition and their influence on supergene Ni products into account (Colin et al., 1990; de Oliveira et al., 1992; Proenza et al., 2008; Talovina et al., 2008; Thorne et al., 2009; Gallardo et al., 2010; Alevizos and Repouskou, 2011; Sagapoa et al., 2011). Other important observations on Ni grade distribution have been made, such as enrichment from the weathering of serpentine minerals (Zeissink, 1969), Ni grade correlation with other metals (Co, Cr, Al, and Fe) concentrated in the residue of laterites (de Vletter, 1978) and the existence of mineralized veins causing high Ni grades (Dowd, 1992).

Rock fracture systems are also important in the enhancement of Ni grade in saprolite layers because they form preferential pathways for dissolved Ni transportation and ultimately precipitation (Pelletier, 1996). Meteorological conditions have also been identified as a key factor in Ni enrichment (de Oliveira et al., 1992; Lewis et al., 2006; Herrington et al., 2007; Thorne et al., 2012).

* Corresponding author.

E-mail addresses: asran_ilyas@yahoo.com (A. Ilyas), kashiwaya.koki.8a@kyoto-u.ac.jp (K. Kashiwaya), koike.katsuaki.5x@kyoto-u.ac.jp (K. Koike).

Nevertheless, the distribution of Ni grade in a deposit, taking into account modeling of the controlling factors, requires more detailed investigation. The purpose of this study is to clarify these issues by spatial modeling of Ni grade using geostatistical techniques, and by considering the effects of topography and paleo-groundwater flow. Two software packages have been used to this end, ArcGIS®Geostatistical Analyst and S-GeMS (Stanford Geostatistical Modeling Software). In addition to borehole data, mineralogical and chemical analysis of soil and rock samples was undertaken using Energy Dispersive X-Ray Spectroscopy (EDX), X-Ray Fluorescence (XRF), X-Ray Diffraction (XRD), and petrographic studies achieved through optical microscopy.

2. Material and methods

2.1. Study area and geological setting

Sulawesi Island in central Indonesia contains one of the richest Ni laterite deposits in the world. Many of the individual deposits are concentrated in the Sorowako area of the South Sulawesi Province (Fig. 1). The international Ni mining company, PT. INCO Indonesia, developed this deposit and has been mining it since 1968. A total of 294 boreholes have been advanced in a lattice pattern along an E–W transect 1.6 km in length, and a N–S transect for 1.0 km across the deposit, to an average depth of 26.62 m below ground level. Within each borehole, metallogenic and chemical compositions were recorded at 1-m intervals (Table 1). The boreholes are spaced at 50-m intervals (Fig. 2), and given the density of geological data thus available, this deposit was selected as the test site for the Ni grade modeling presented here.

Sulawesi Island is situated at a triple junction of three tectonic plates; the Indo-Australian plate, the Pacific plate, and the Eurasian plate. The plate movements of these have been tracked as towards the north, west and south-southeast, respectively. The generation of the Ni laterite deposits is closely related to these convergent plate movements, given the development of active faulting, extensional basins

Table 1

Borehole sample data indicating depth, Ni, Fe, SiO₂ and MgO content, layer and rock type, and mineralogy. The depth ranges of data at all sites were classified into three layers: limonite, saprolite, and bedrock.

Drillhole number	Depth range (m)	Ni (wt.%)	Fe (wt.%)	SiO ₂ (wt.%)	MgO (wt.%)	Layer	Rock type	Primary mineral
A103966	0.20–1.00	1.04	45.20	7.80	1.50	lim		hmt
A103966	1.00–2.00	1.03	47.70	6.50	1.30	lim		hmt
A103966	2.00–3.00	1.09	48.80	5.70	1.20	lim		hmt
A103966	3.00–4.00	1.02	48.80	5.40	1.30	lim		hmt
A103966	4.00–5.00	1.18	46.90	6.40	1.60	sap		hmt
A103966	5.00–6.00	1.25	44.00	8.60	1.60	sap		hmt
A103966	6.00–7.00	0.29	7.30	34.70	41.20	sap		olv
A103966	7.00–7.90	0.29	7.20	26.70	30.60	bdr	hrz	olv
A103966	8.00–9.00	0.32	8.20	23.60	27.00	bdr	hrz	olv
A103966	9.00–10.00	0.29	7.10	27.30	31.50	bdr	hrz	olv
A103966	10.00–11.00	0.32	8.90	29.00	31.90	bdr	hrz	olv

lim: limonite, sap: saprolite, bdr: bedrock, hrz: harzburgite, hmt: hematite, olv: olivine.

and generally complex geological structures throughout the Cenozoic (Macpherson and Hall, 2002). The ‘K’-shape of Sulawesi Island is attributed to four principal lithotectonic belts, which are bounded by large-scale tectonic dislocations and comprise the West Sulawesi Volcano-Plutonic Arc Belt, the Central Sulawesi Metamorphic Belt, the East Sulawesi Ophiolite Belt, and the continental fragments of Banggai-Sula, Tukang Besi, and Buton (Fig. 1) (Mubroto et al., 1994; Kadarusman et al., 2004). The study area is located in the East Sulawesi Ophiolite Belt in which Cretaceous ultramafic rocks crop out because of subduction processes which occurred in the Miocene, approximately 10 Ma ago (Golightly, 1979; Suratman, 2000).

The Sorowako area is composed mainly of three rock units: Quaternary alluvial deposits and lacustrine deposits, Tertiary ultramafic rocks such as harzburgite in which the Ni laterite deposits are hosted, and Cretaceous sedimentary rocks (Golightly, 1979; Suratman, 2000). Most deposits are located in hill and low mountain topographic regions

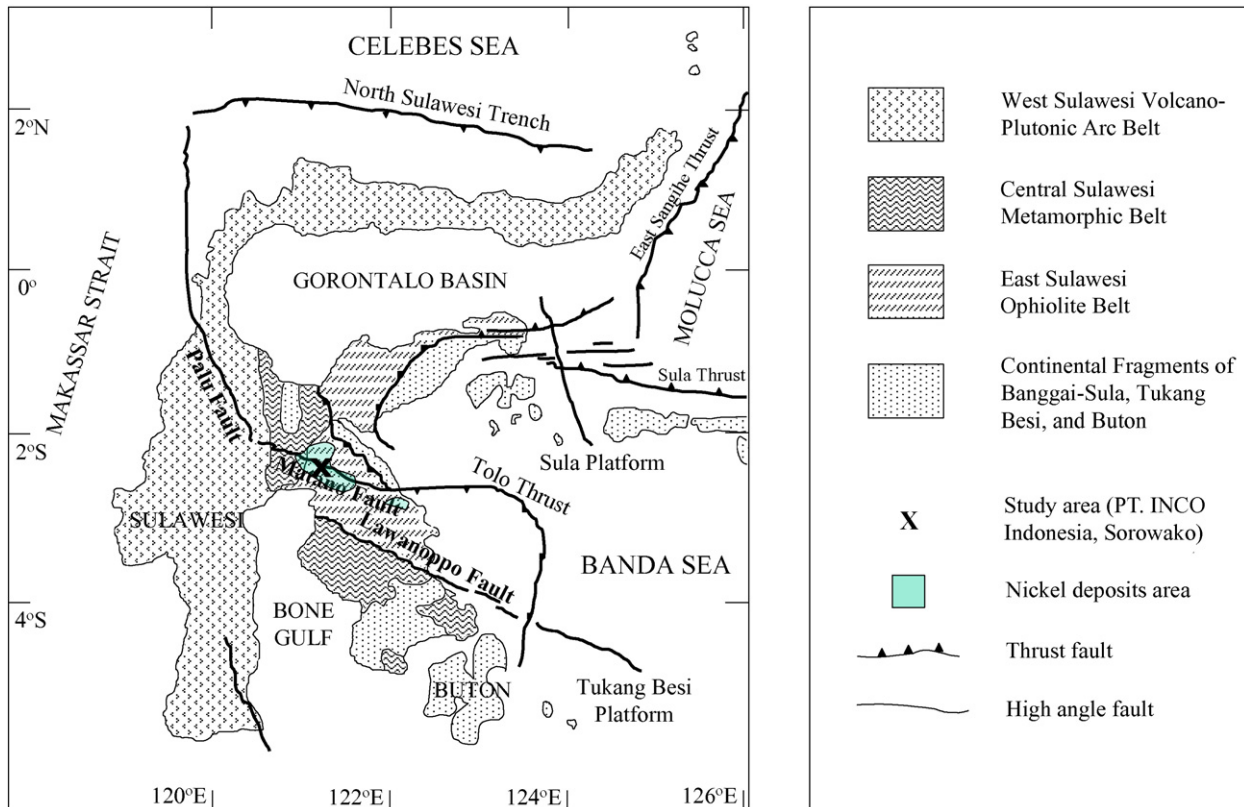


Fig. 1. Location of the study area (marked with an X) in South Sulawesi Province, Sulawesi Island, Indonesia, indicating the four principal tectonic belts and overall geological structure.

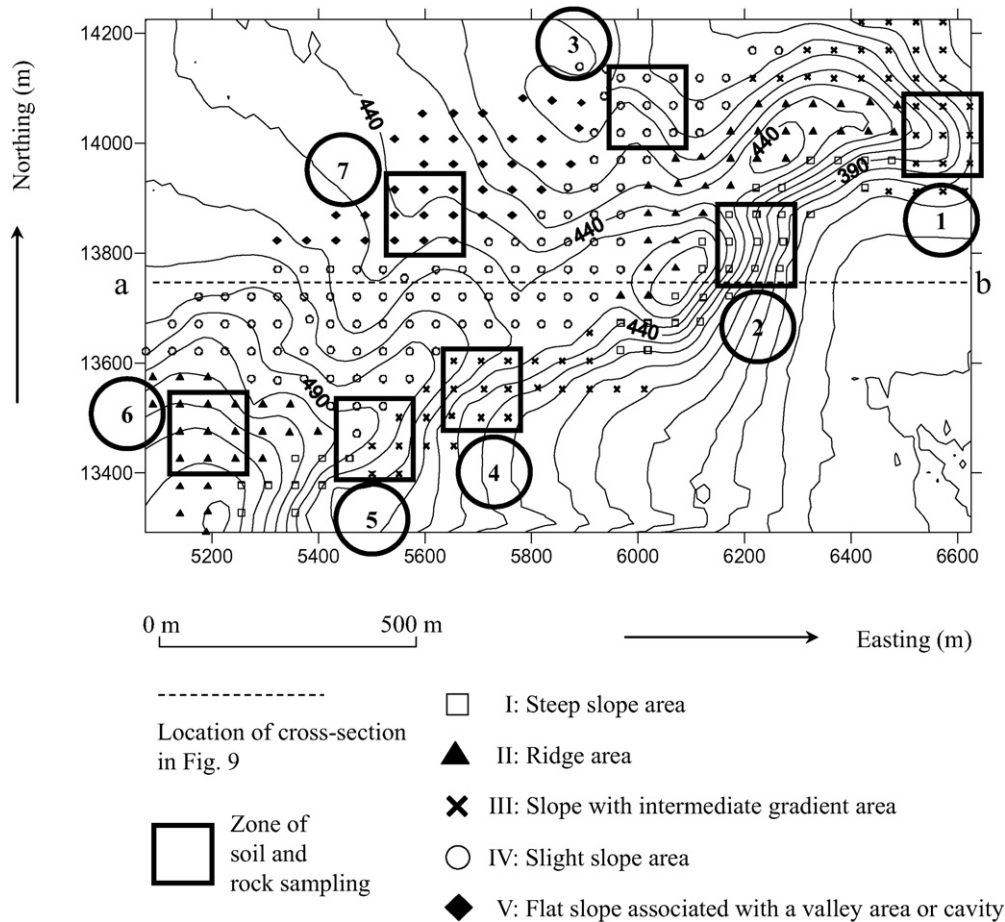


Fig. 2. Topographic map of the study area indicating the distribution of 294 boreholes along the 1.6 km (E–W) and 1.0 km (N–S) directions used for Ni exploration. The sites are variously depicted by five symbols according to five topographic categories. This map includes the seven zones of differing topography selected for soil and rock sampling at the center of each zone. Topographic categories are I: steep slope (Zone 2), II: ridge area (Zone 6), III: intermediate slope (Zones 1 and 4), IV: slight slope (Zones 3 and 5) and V: flat slope associated with a valley area or cavity (Zone 7).

that formed during deep erosion and strong weathering of serpentinized and unserpentinized ultramafic rocks.

The study area is generally composed of unserpentinized harzburgite and dunite bedrock (Fig. 3) whose original Ni contents range from 0.10 to 2.88 wt.% with the average 0.53 wt.% (PT. INCO

Indonesia, 2006). The Ni laterite deposits of the study area are classified as hydrous silicate type containing harzburgite and dunite. The upper horizons of the bedrock are well fractured with garnierite and other silicates present in the fractures (PT. INCO Indonesia, 2006). The weathered strata above the bedrock comprise two layers: a limonite layer near

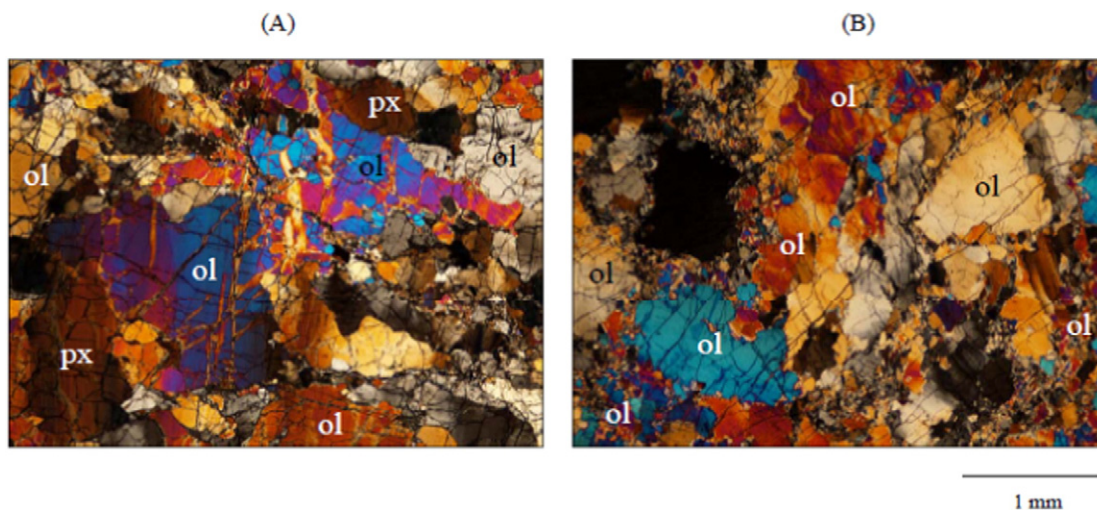


Fig. 3. Photomicrographs of typical basement rocks in the study area (crossed nicols). A. Harzburgite, composed mainly of olivine (ol) and pyroxene (px). B. Dunite, composed mainly of olivine.



Fig. 4. Typical outcrop of the limonite layer, the saprolite layer below it, and the undulative boundary between the two layers.

the surface and a saprolite layer below it as shown by a typical outcrop photo (Fig. 4), both of which have an average thickness of 11 m (PT. INCO Indonesia, 2006). Fine-grained red, brown, and yellow soils constitute the limonite layer which thins under the steep slopes and can be absent because of deep erosion. Goethite is the main Ni containing mineral in the limonite, which occurs via the replacement of Fe by Ni.

The saprolite layer, brownish yellow in color, is a mixture of soil and unweathered host rock that retain their original texture and structure. Some layers contain fine-grained limonite remnants, saprolitic rims, garnierite veins, nickeliferous quartz, manganese, and silica boxwork structures. This layer is well fractured, and weathering is enhanced by groundwater ingress through the fractures, resulting in spheroidal development of the host rock between fractures and Ni-bearing garnierite

forming rims to the spheroidal rock. The fractures are typically filled with secondary chlorite and quartz.

2.2. Sample data and geostatistical analysis

Geostatistics has been successfully applied to ore grade estimation and modeling in many mineral deposits (Koike et al., 1998; Srivastava, 2005; Verly, 2005; Emery, 2006; Ilyas and Koike, 2012; Sadeghi et al., 2015). The reason of adopting geostatistics was its advantages of geostatistics over spline-based spatial interpolators such as the minimum curvature (Briggs, 1974) and the spline with tension (Mitasova and Mitas, 1993), which can mainly implement 3D modeling, consider

Table 2

Criteria used to define topographic categories I to V based on slope gradient, the number of boreholes, and the main location for each category.

No.	Topographic category	Slope gradient	Number of drillholes	Location
I.	Steep slope area	$\geq 45^\circ$	37	East and Southwest sides
	Ridge area (regions near the line of a ridge)	$20^\circ\text{--}44^\circ$ (at topography near the line of a ridge near the top of a hill)	55	Northeast and Southwest sides
II.	Slope with intermediate gradient area	$20^\circ\text{--}44^\circ$	58	Northeast and South sides
IV.	Slight slope area	$5^\circ\text{--}19^\circ$	105	Central, West, and North sides
V.	Flat slope associated with a valley area or cavity	$<5^\circ$	39	Northwest side

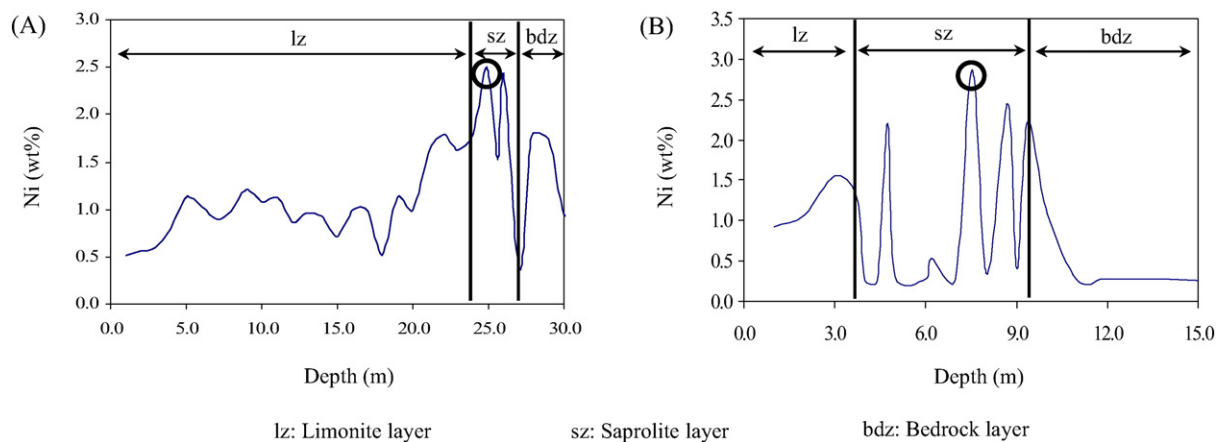


Fig. 5. Depth-dependent changes in Ni grade in the limonite, saprolite and bedrock layers measured at two borehole sites. A. Site located on slight slope topography. B. Site located on ridge topography. In both cases, the maximum Ni grade occurs in the saprolite.

anisotropic behavior of the Ni content data, and produce more complicated spatial model by considering local change in the data values.

The sample data set of Ilyas and Koike (2012) was used to prove the presence of a spatial correlation with Ni grade and here the use of geostatistics is applied for the same purpose. Following Ilyas and Koike (2012), the topography of the study area was divided into five categories (see Fig. 2): (I) steep slope areas (gradient $\geq 45^\circ$), (II) ridge areas (regions near the line of a ridge with gradient $< 45^\circ$), (III) slopes with intermediate gradient (gradient $\geq 20^\circ$), (IV) slight slopes (gradient $\geq 5^\circ$) and (V) flat slopes with a gradient $< 5^\circ$ typically associated with a valley or cavity feature, depending on the slope angle (Van Zuidam, 1985). Table 2 summarizes the characteristics of each topographic category.

2.3. Chemical and mineralogical analysis

To clarify the chemical and mineralogical factors that control the Ni grade at the sample scale, soil and rock samples were taken from seven sites (each 100×100 m) near the boreholes. Six samples were retrieved at each site, two each from the limonite, saprolite and bedrock layers. Each sample site was near the borehole location at the center of seven selected zones (Zones 1 to 7) as shown in Fig. 2. These locations were chosen based on the soil and rock outcrops displaying the appearance of laterization layers in the field.

Chemical and mineralogical compositions were analyzed as follows. The four main elements of peridotite rocks (Ni, Fe, Si, Mg) were measured by a handheld XRF (JEOL, DELTA, Element Analyzer) and an EDX with scanning electron microscope attached (JEOL, JSM-6510A). This was done to investigate the relationship between their mineral content, degree of weathering and the difference in Ni grade between the limonite and saprolite in detail. The main constituent minerals were identified by XRD (Shimadzu, X-Ray Diffractometer-6000) and optical microscopy was also used for mineralogical assessment of the bedrock samples (Fig. 3).

3. Results

3.1. Effect of topography on Ni grade

To understand the correlation between the topographic category and Ni grade from the surface to bedrock, Ni grades from two boreholes from the slight slope (Fig. 5A) and ridge areas (Fig. 5B) were selected. Common to both categories, the Ni grade increases gradually with depth in the limonite layer, fluctuates largely in the saprolite layer (in which the maximum grade was recorded), and decreases toward the bedrock layer. The grades in the bedrock layer are generally lower than those in the saprolite layer. Scattergrams of the thickness of laterization layers plotted against the topographic category indicate that the mean thickness of the limonite layer tends to increase from steep to flat topography (category I to V), as shown by a regression line, while the mean thickness of the saprolite layer does not correlate with the topographic slope (Fig. 6).

3.2. Selection of a geostatistical method

To choose a geostatistical method suitable for Ni grade modeling, the correlations between Ni grade and the concentrations of Fe, SiO₂ and MgO were investigated. A method for single variable or multivariate analysis is used depending on the absence or presence of correlation, respectively, which is evaluated by a coefficient of determination (R^2). The R^2 values are low over all the combinations common to the limonite, saprolite, and bedrock layers. The maximum value is only 0.25 for the Ni and Fe pair in the bedrock (Table 3).

Similarly to the aspects of topography and layer thickness, the relationship between Ni grade and slope angle, and between Ni grade and the saprolite layer thickness, was examined, primarily because the

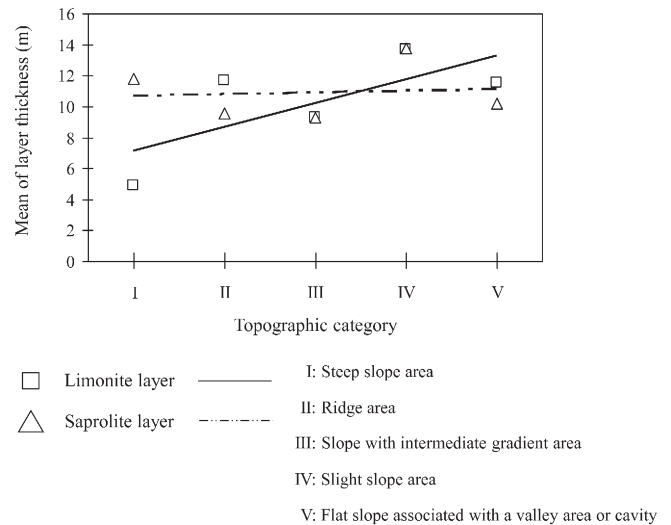


Fig. 6. Graphic illustration of the relationship between the topographic category and the mean thickness of the laterized layers (limonite and saprolite layers), indicating that trend in limonite layer thickness increases from topographic categories I to V.

maximum Ni grade was recorded in the saprolite. However, these relationships are absent, as shown in Fig. 7.

The general lack of correlation between the Ni grade and other chemical, topographic, and geological factors necessitated the use of geostatistical methods for investigating single variables, namely variography and ordinary kriging. Spatial correlation of the Ni grade was characterized by experimental semivariogram analysis under the assumption of an orthogonal anisotropy in both horizontal and vertical directions. Calculation of the horizontal semivariogram was omnidirectional because the numbers of data pairs were biased with respect to the distribution of the boreholes (Fig. 2) given that there were fewer pairs in a NW–SE direction than along the main axis in a NE–SW direction. Correct characterization of anisotropic behavior in the horizontal direction was therefore difficult. The experimental semivariograms were approximated by a spherical model for both directions as shown by the curves superimposed in Fig. 8, because the model was found to be the best fit among the typical semivariogram models such as the exponential and Gaussian models. The maximum correlation lengths along the horizontal and vertical directions were found to be 280 m (Fig. 8A) and 10 m (Fig. 8B), respectively.

3.3. Ni grade distribution

Ni grade distribution was modeled in 3D to a maximum depth of 50 m using the above-mentioned semivariograms and ordinary kriging as shown in Fig. 8. The Ni grade ranges from 0.23 to 2.0 wt.% and the local distributions of high-grade zones (> 1.56 wt.%) near the ground surface and near the bottom boundary are shown in Fig. 9. The value

Table 3
Correlation coefficients for Ni vs. Fe, Ni vs. SiO₂, and Ni vs. MgO for each laterized layer.

Laterization layer	Correlation between chemical concentrations	Coefficient of determination (R^2)
Limonite	Ni vs Fe	0.05
	Ni vs SiO ₂	0.08
	Ni vs MgO	0.02
	Ni vs Fe	0.18
Saprolite	Ni vs SiO ₂	0.01
	Ni vs MgO	0.23
	Ni vs Fe	0.25
Bedrock	Ni vs SiO ₂	0.01
	Ni vs MgO	0.20

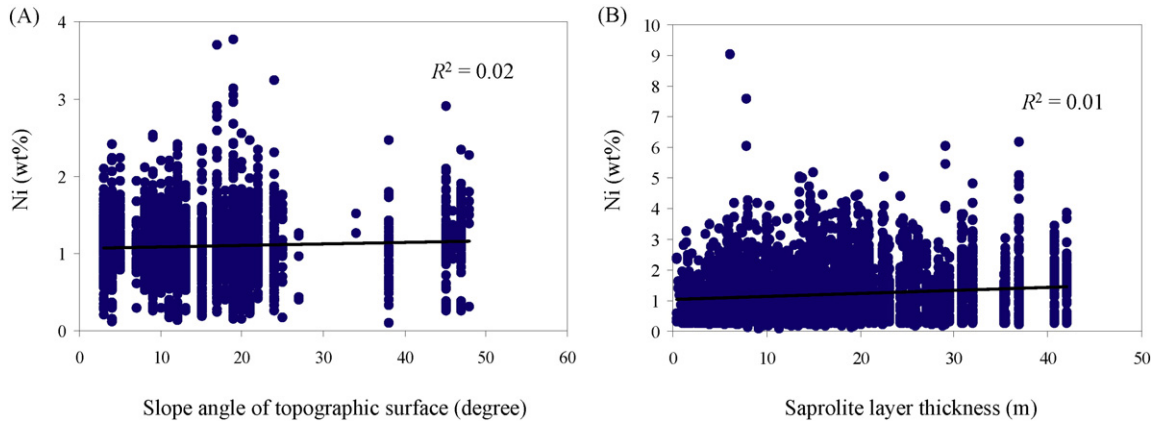


Fig. 7. Scattergrams showing the relationship between slope angle, layer thickness and Ni grade. A. Slope angle vs. Ni grade in the limonite layer. B. Saprolite layer thickness vs. Ni grade. Both graphs indicate a complete lack of correlation.

of 1.56 wt.% for high grade was defined as the values from the 4th quartile.

The locations of high-grade zones are characterized by their relationship with topography, as depicted in Fig. 10 along with an E–W cross-section of the 3D Ni grade model that passes through the highest grade zones and three topographic categories: IV: slight slope, II: ridge and I: steep slope. Two noteworthy trends are that the high-grade zones are generally located in two depth ranges – the shallow range from the surface to 10 m below ground level (mainly in the limonite layer) and the deep range from 20 to 40 m below ground level (mainly in the saprolite layer) – and that zones are distributed below slight slopes (category IV).

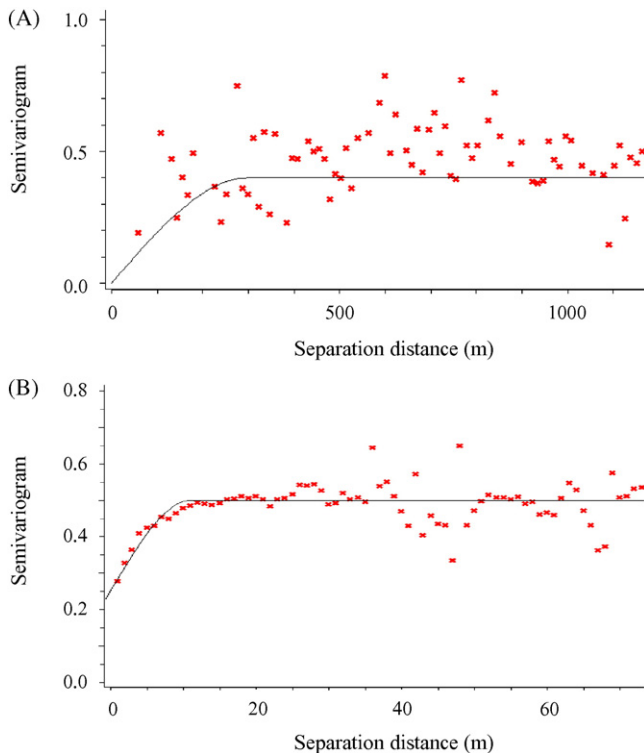


Fig. 8. Experimental semivariograms of Ni grade data and their approximation by the spherical model. A. Omnidirectional horizontal plane. B. Vertical plane.

3.4. Chemical and mineralogical composition

Despite the spatial distribution of samples, the Ni and Fe contents are nearly identical throughout, as evidenced from the XRF and EDX data (Table 4). With the exception of the Zone 5 sample, the Ni content is higher in the limonite layer than in the saprolite layer. The highest Ni content was recorded in the sample from the saprolite layer of Zone 2 where dunite forms the bedrock.

Two XRD patterns for samples from the limonite and saprolite of Zone 3 are presented in Fig. 11A and B, respectively, and highlight goethite and quartz as the main constituent minerals. Importantly, goethite was identified in both the limonite and saprolite layers common to the seven zones (Table 5). Goethite is a secondary mineral, typically generated by the reaction of ground-water and iron-bearing minerals during weathering of ultramafic rocks.

As a result, and because the present groundwater table is in the bedrock layer, goethite may have been generated in a paleo-groundwater system in the laterization layer. Hence the paleo-groundwater system can be considered as a mechanism by which Ni was dissolved and transported during laterization.

4. Discussion

4.1. Estimation of the paleo-groundwater system

The most important factor that has controlled weathering of the peridotite basement in the study area is water–rock interaction. This interaction can be considered as groundwater flow through fractures, fissures and faults, as well as interconnected pore spaces, resulting in eventual dissolution of the surrounding rocks, which further results in soil development when coupled with the influences of humic acids near the ground surface (de Vletter, 1978; Cluzel and Vigier, 2008). The development of fractures were observed in particular in the saprolite layer, which is shown by the two outcrop photos around the Zone 2 in the steep slope area (category I) (Fig. 12A) and around the Zone 7 in the flat slope associated with a valley area or cavity (category V) (Fig. 12B). The water–rock interaction through the fractures over a long duration, with potentially large quantities of groundwater, advanced the weathering process and consequently formed thick laterization layers (limonite and saprolite). Additionally, closely spaced fractures or joints would cause large circulation of groundwater and create rich concentration of garnierite and thick laterite layer (Robb, 2005).

The water–rock interaction dissolved Ni-bearing minerals, transported the Ni, and precipitated the Ni by supergene processes. In

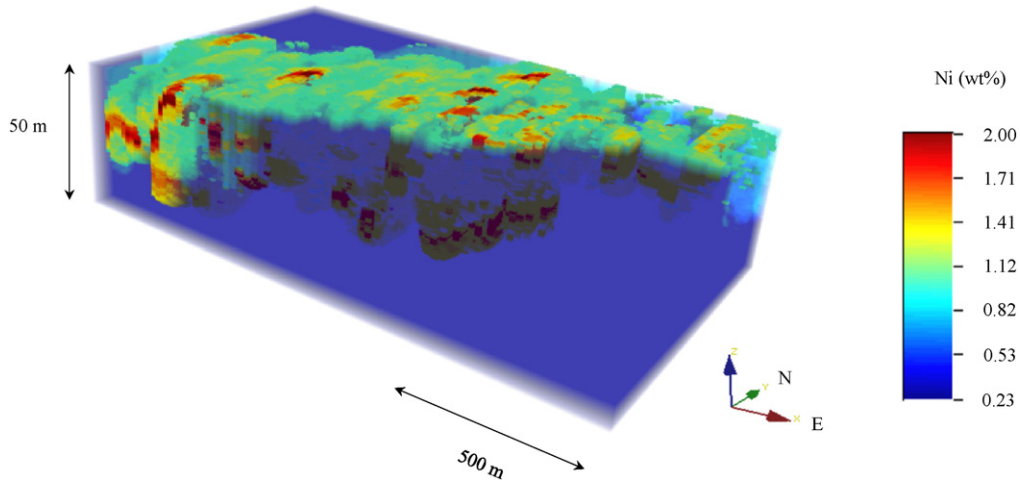


Fig. 9. Ni grade distribution produced by ordinary kriging in a 3D model (viewed from the southeast). The blue color on the surfaces of the model denotes those zones far from the borehole sites and outside of the calculations.

the long-term, groundwater in the limonite layer flowed horizontally or migrated vertically (Sagapoa et al., 2011) into the saprolite layer. As a result, Ni has generally been enriched in the saprolite layer; i.e. in the ultramafic rocks via impregnation from a Ni-rich groundwater solution. This enrichment has an original relationship with the parent rocks such as harzburgite and dunite (Kubo, 2001): higher content of Ni in the rocks, particularly in olivine, can cause stronger enrichment.

Olivine and pyroxene, which are main constituent minerals of the ultramafic rocks, are changed to serpentine, a hydrous magnesium silicate, by the weathering. Conversely, olivine is generated from serpentine. These reactions are:

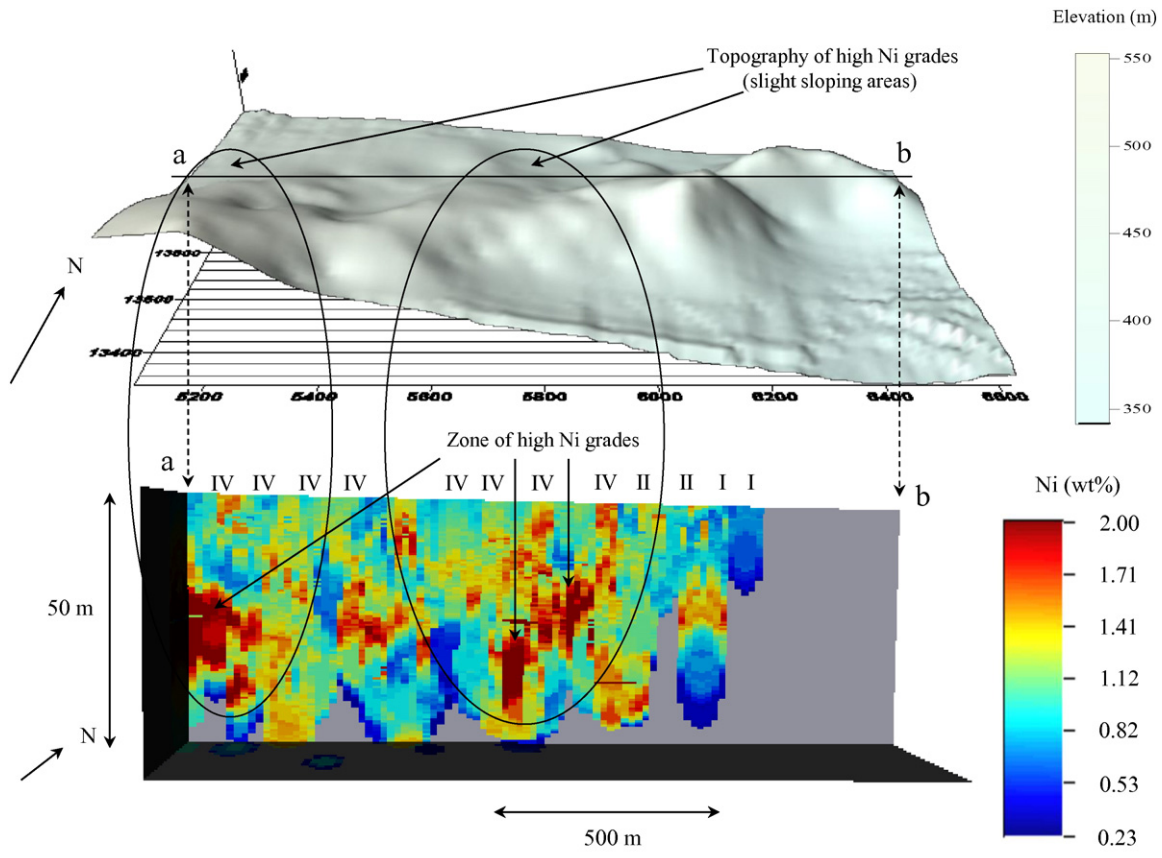
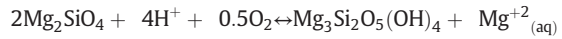


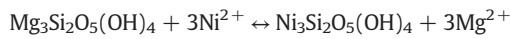
Fig. 10. Cross-section along the E–W direction of the Ni grade distribution model shown in Fig. 9, highlighting that the high Ni grade zones tend to be formed below the category IV slopes (5–19° gradient) and the change in Ni grade with the change in topographic category (IV, II, and I: see Table 2) shown at the top of cross-section from west to east (a to b). Location of cross-section is shown in Fig. 2.

Table 4

Tabulated XRF and EDX data for limonite and saprolite layer samples per zone, and indicating the main mineralogy and bedrock type identified. The samples were taken from outcrops near the central borehole in each zone (see Fig. 2).

Zone	Laterization layer	XRF element analysis (%)				EDX analysis (%)				Bedrock	Bedrock minerals
		Ni	Fe	Si	Mg	Ni	Fe	Si	Mg		
1	Limonite	0.93	46.00	3.55	1.95	0.93	45.70	8.26	0.97	Harzburgite	Olivine, pyroxene
	Saprolite	1.47	43.61	4.45	2.22	1.59	43.60	10.14	1.37		
2	Limonite	0.84	54.13	1.40	1.65	0.91	48.88	2.83	0.71	Dunite	Olivine, metallic minerals
	Saprolite	2.10	49.33	3.50	1.53	2.36	44.95	6.37	1.66		
3	Limonite	0.76	53.30	0.94	2.78	0.73	52.39	1.06	0.40	Harzburgite	Olivine, pyroxene
	Saprolite	1.03	44.85	4.67	1.46	1.12	48.63	7.74	0.74		
4	Limonite	1.21	53.47	1.30	2.14	1.15	54.62	3.00	0.55	No sample	No sample
	Saprolite	1.73	45.00	2.50	2.14	1.35	47.17	7.01	0.63		
5	Limonite	0.75	50.24	1.86	2.04	0.98	49.42	5.36	0.50	Harzburgite	Olivine, pyroxene
	Saprolite	0.49	30.10	3.72	1.90	0.95	40.66	7.96	4.56		
6	Limonite	1.78	36.78	6.19	1.54	1.81	30.35	15.36	5.49	Harzburgite	Olivine, metallic minerals
	Saprolite	1.27	39.60	3.38	1.56	2.02	42.02	8.64	3.71		
7	Limonite	0.60	53.55	1.54	2.84	0.79	54.11	4.34	0.71	Harzburgite	Olivine
	Saprolite	1.08	45.46	3.22	1.75	1.40	47.06	7.28	2.97		

For the case of hydrosilicate minerals, Ni replaces the Mg atoms, as shown in serpentine, as an example, by the following reactions (Gallardo et al., 2010).



Serpentine usually contains small amounts of Ni, cobalt, and chromium, which causes the concentration of Ni in the iron-rich laterites and formation of Ni ores (Guilbert and Park, 1986). Alternatively, precipitation of a Mg- and Si- rich solution occurs in open fractures as supergene garnierite that typically precipitates in the lower parts of the weathered

ultramafic profiles and ranges from green to yellow-green in color (Soler et al., 2008).

Because the thicknesses of the limonite and saprolite layers can be used as a reasonable indicator of the paleo-groundwater system, they were subjected to geostatistical analysis. The key assumption in interpreting their distribution is that the layers became thickest along the paleo-groundwater flow region where water-rock interaction was longest in duration (Evans, 1987). Assuming that groundwater flow tends to approximate topographic slope, i.e. from high to low elevation, it can be conjectured that the weathered layer becomes thickest in a downstream direction, supported by the likely decrease in flow velocity

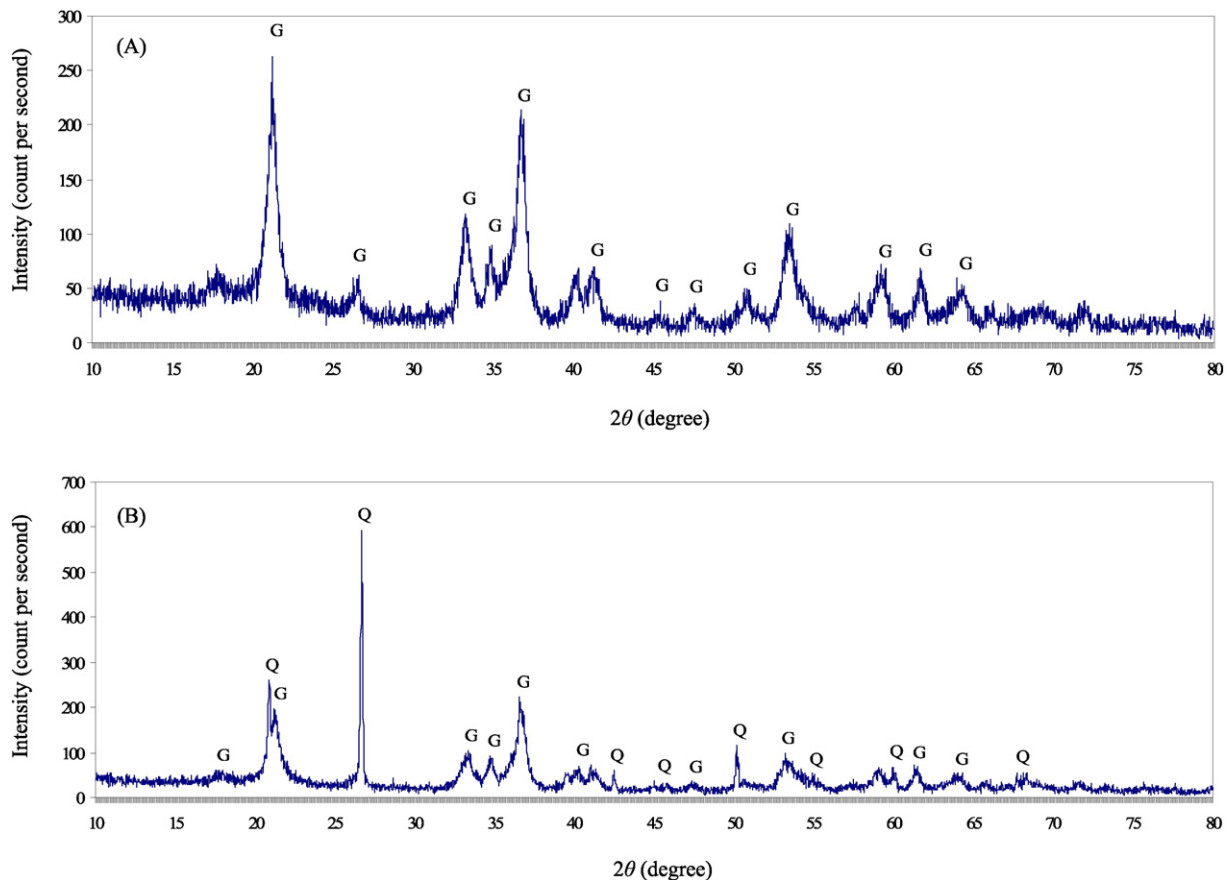


Fig. 11. XRD patterns of soil samples. A. Limonite sample from Zone 3. B. Saprolite sample from Zone 3. Both patterns indicate the main constituent minerals are goethite (G) and quartz (Q).

Table 5

Main minerals identified by XRD analysis in the limonite and saprolite layers from each of the seven zones (Fig. 2) based on the soil samples presented in Table 4.

Zone	Laterization layer	Main minerals from XRD analysis
1	Limonite	Quartz, goethite
	Saprolite	Quartz, goethite
2	Limonite	Pyrolusite, goethite
	Saprolite	Tremolite, goethite
3	Limonite	Goethite
	Saprolite	Quartz, goethite
4	Limonite	Goethite
	Saprolite	Forsterite, goethite
5	Limonite	Goethite
	Saprolite	Enstatite, goethite
6	Limonite	Hornblende, goethite, asbolane
	Saprolite	Goethite, hornblende
7	Limonite	Goethite, cochromite
	Saprolite	Hornblende, goethite

beneath shallower topography which results in an increased duration of water–rock interaction. Although the weathered layers have undergone erosion and their original thicknesses have likely changed, their relative thicknesses may have been preserved where erosion rates were slow relative to the rate of chemical weathering (Brand et al., 1998). To analyze the local groundwater flow direction and its relationship to the Ni grade distribution in detail, seven small areas (Zones 1 to 7) containing nine borehole sites each, were selected (Fig. 2).

As shown in Table 1, the boundary of limonite and saprolite layers was defined only on the basis of four chemical constituents and mineralogy. Additionally, the thicknesses of these layers could not be correctly determined because of core losses in the strongly weathered rocks during drilling. The length percentage of core losses over the total borehole length at each site ranges from 5 to 10%. To estimate the true thicknesses, vertical semivariograms of the Ni, Fe, SiO₂, and MgO contents along the depth direction were produced for each individual borehole site in each zone. Because these contents were different between the two layers and the core losses were not severe as above, correlation length of the contents, which is equal to the semivariogram range, is the only available indicator of the layer thickness.

Fig. 13 shows examples of the semivariograms for each constituent at the center of Zone 2. Common to the four elements, the semivariograms can be approximated by a spherical model and the ranges are similar: Ni = 3.7 m, Fe = 3.6 m, SiO₂ = 4.7 m and MgO = 2.8 m. The average of the ranges can then be taken as the thickness of the limonite layer because of the long-term weathering from ground surface to bedrock, which must have generated a spatially correlated distribution of chemical constituents. This range identification and averaging was repeated for all the boreholes. The top of the bedrock identified in the original data was deemed to be accurate because they are

consolidated unlike the unconsolidated limonite and saprolite layers. The thickness of the saprolite layer was obtained simply by subtracting the averaged thickness of limonite layer from the depth of the top of the bedrock.

Next, the thicknesses of limonite and saprolite layers were interpolated individually in each zone by producing omnidirectional horizontal semivariograms of the nine datasets and applying ordinary kriging. Fig. 14 shows examples of the semivariogram maps, depicting the binning process in the production of the experimental semivariogram, and the two resultant thickness distributions for Zone 2. Each cell in Fig. 14B and D expresses the semivariance of the data pairs with the same separation distances along the E–W and N–S directions. For the present data distribution (Fig. 14A), only separation distances of 0 m, 50 m and 100 m are defined along each direction, and diagonal quadrants are symmetrical.

To identify the paleo-groundwater flow direction, two conditions were set: the flow occurred from (i) the smallest to the largest semivariances and from (ii) the thinnest toward the thickest layers, as determined by ordinary kriging. The direction that satisfied both these conditions was selected.

The thickness of the limonite layer ranges from 2.49 to 5.97 m and that of the saprolite layer ranges from 0.30 to 11.77 m in Zone 2. It is evident that spatial trends in thickness appear in both layers (Fig. 14C and E). The limonite layer tends to thicken from the south to the north (Fig. 14C) which is concordant with the south to north increase in semivariances (Fig. 14B). Therefore, the paleo-groundwater is estimated to have flowed from south to north. In the saprolite layer it is evident that the directions which satisfy conditions (i) and (ii) are southwest to northeast (Fig. 14D and E) and the paleo-groundwater flow in this layer is therefore estimated to have been in this direction. The averaged direction of the two layers, SSW–NNE is taken to be the resultant flow direction for Zone 2 (Fig. 14F).

It can also be noted that the two flow directions estimated in the two layers, particularly in the saprolite, correspond roughly with the SW–NE orientated ridge line.

The estimation of paleo-groundwater flow in the limonite and saprolite layers was applied to all the zones and, from the flow direction map, it appears that most directions seem to be roughly parallel to the topographic contour lines and not along the present dip directions (Fig. 15A). However, the flow in Zones 3 and 4 are directed to currently higher elevations, suggesting that the paleo-topography may have been largely different to that of the present.

To check the correlation between paleo-groundwater flow direction and Ni grade, the estimated directions are compared with the 3D Ni grade distribution from an E–W cross-section through Zone 7, parallel to the estimated flow direction (E–W) in this Zone (Fig. 15B). It can be observed that the Ni grades increase from relatively low grades (<0.5 wt.%) to one of the highest grades (>1.4 wt.%) along the paleo-

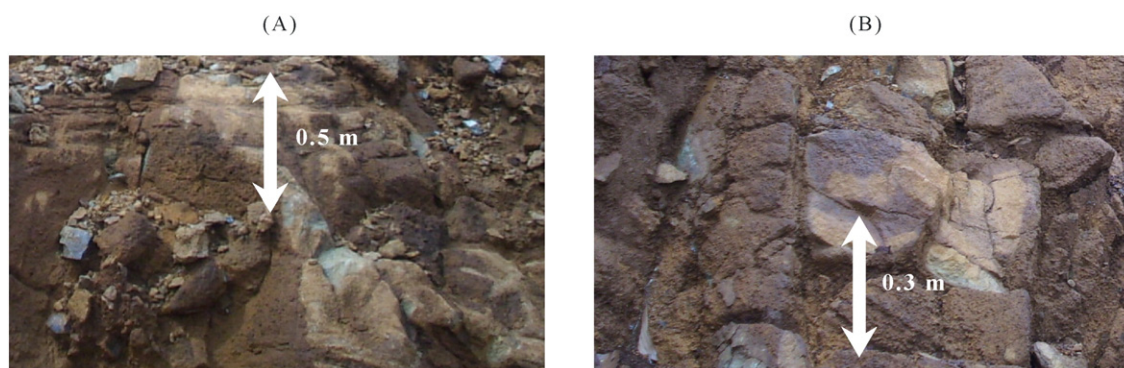


Fig. 12. Typical outcrops showing the development of fractures in the saprolite layer around the Zone 2 in the steep slope area (category I) (A) and around the Zone 7 in the flat slope associated with a valley area or cavity (category V) (B).

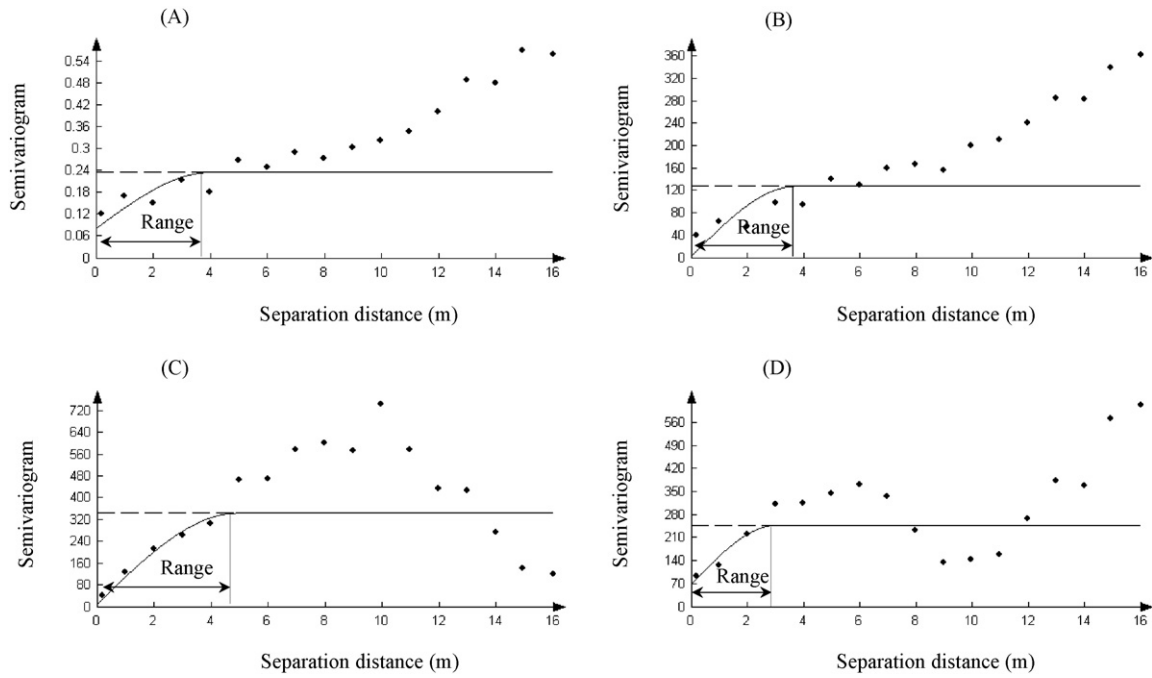


Fig. 13. Examples of vertical semivariograms for the limonite layer from the center of Zone 2, used for calculating layer thickness. A. Ni. B. Fe. C. SiO₂. D. MgO.

groundwater flow direction. This is supportive of the above described mechanism of water–rock interaction and Ni transport and precipitation in this deposit.

Further verification is evident from two horizontal cross-sections of the Ni distributions on which the estimated paleo-groundwater flow directions at depths of 11 m and 19 m are superimposed because the

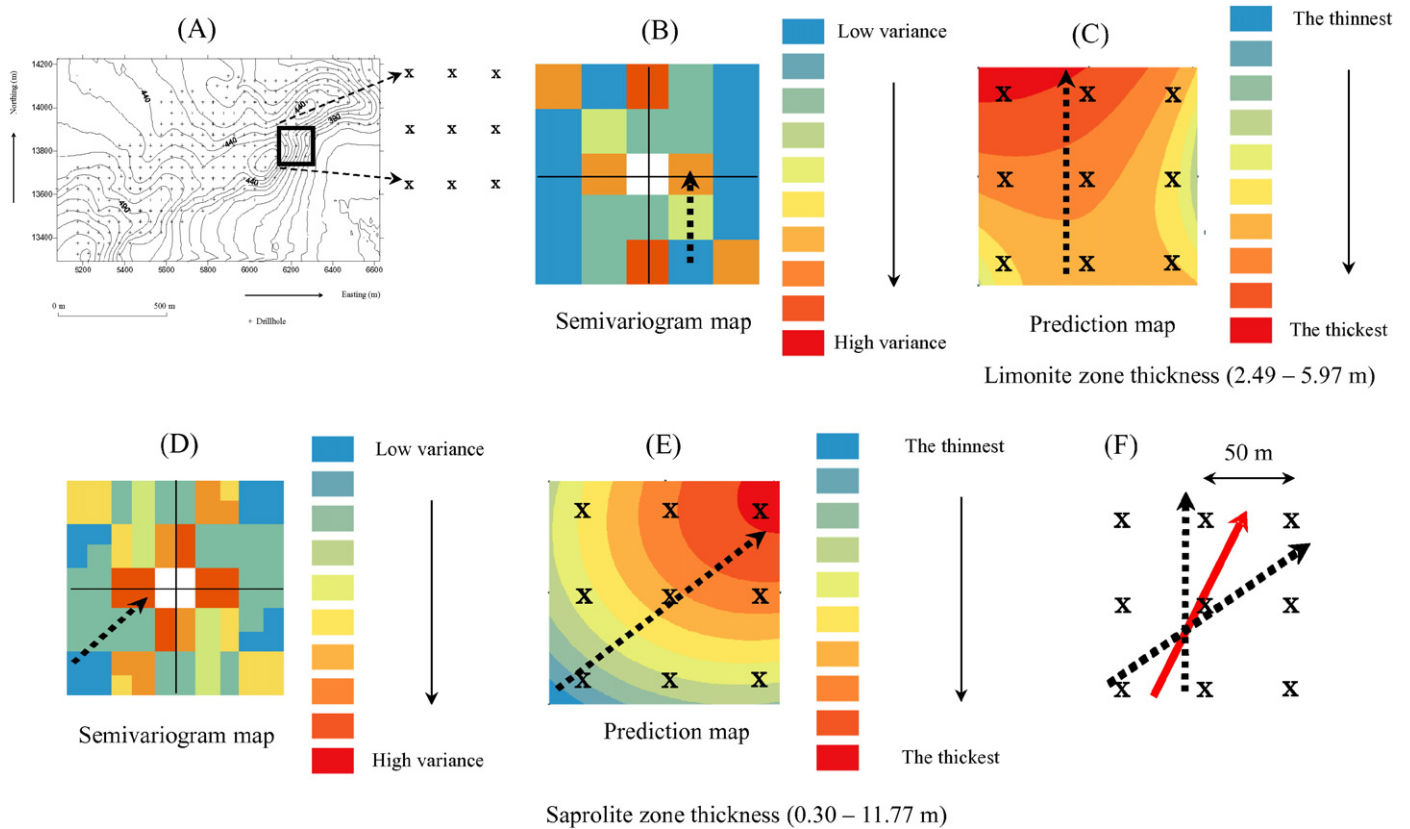


Fig. 14. Illustration of the process for estimating paleo-groundwater flow direction, using Zone 2 as an example. A. Map showing the positions of the nine boreholes in Zone 2. B. Semivariogram map of the limonite layer thickness. C. Thickness distribution of the limonite layer over Zone 2 determined by ordinary kriging. D. Semivariogram map of the thickness of the saprolite layer. E. Thickness distribution of the saprolite layer. The dotted arrows denote the directions along which the semivariograms of thickness increase from low to high (B and D) and the thicknesses increase from thin to thick (C and E). The red arrow in F indicates the composed paleo-groundwater direction vector from those found in the limonite and saprolite layers in Zone 2.

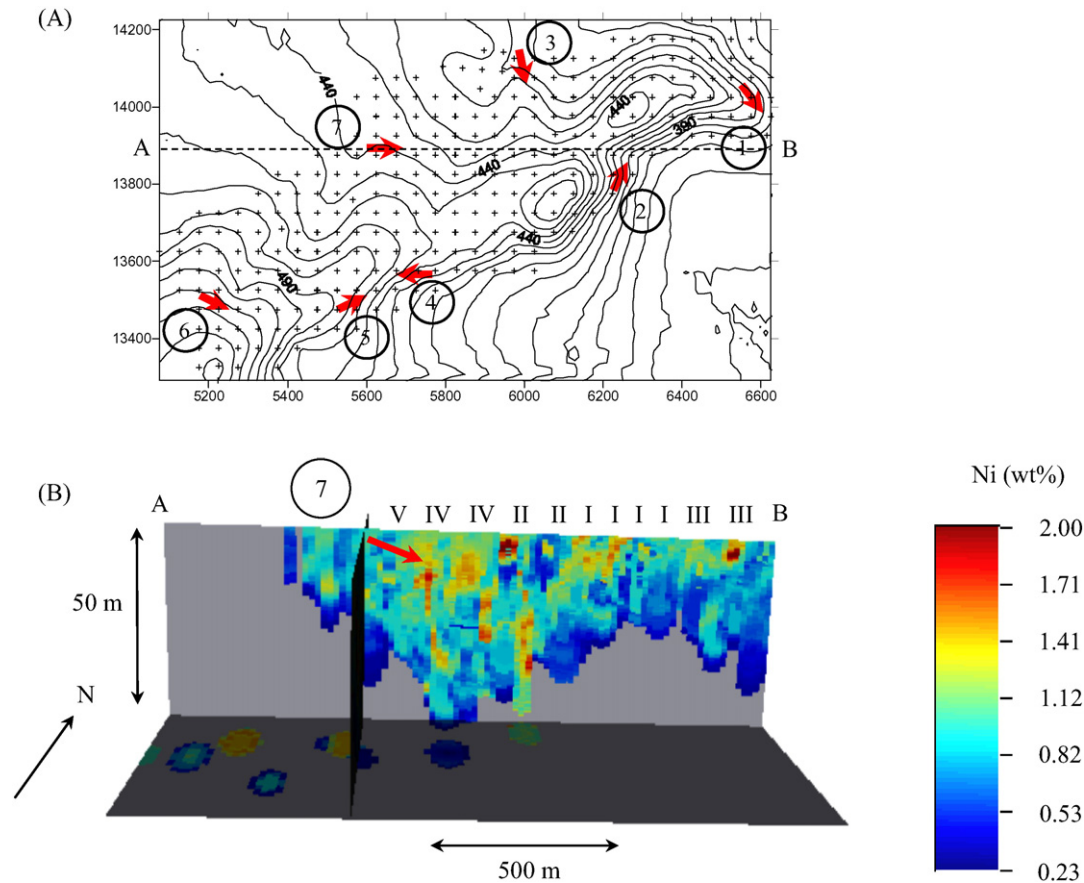


Fig. 15. A. Paleo-groundwater flow directions estimated in Zones 1 to 7, following the process shown in Fig. 14. B. Cross-section of the Ni grade distribution model (Fig. 9) passing through Zone 7 along line A–B. The red arrows indicate the paleo-groundwater flow directions in 3D, interpreted from the directions along which low Ni grades increase to relatively high grades.

highest Ni grades were recorded at these depths (Fig. 16A and B, respectively). The distributions and directions around the seven zones are shown in detail and enlarged in Fig. 17. At both depths, the estimated paleo-groundwater flow is generally parallel to the directions of increasing Ni grades in all the zones.

4.2. Ni accumulation mechanism

Harzburgite, chiefly composed of olivine and pyroxene (~80%), constitutes the bedrock in the study area. These minerals (olivine and pyroxene) are the source of Ni with 0.1 to 0.3 wt.% content and their alteration by hydration can increase the Ni content up to ten times of the original (Robb, 2005). Petrographic analysis indicates the presence of significant fracturing that has developed (Fig. 3A) under the influence of the long-term tectonic processes that have affected the Sorowako area, central Sulawesi Island, Indonesia. The existence of fractures and cracks facilitated enhanced weathering of olivine, which is unstable in the weathering environment, near the Earth's surface (Thorne et al., 2009).

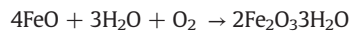
Solubility and mobility of Ni in usual groundwater are small in the presence of soluble elements such as Si and Mg, but Ni is partly soluble in acidic groundwater at low pH (Guilbert and Park, 1986). As a result, Ni has been enriched from multiple cycles of leaching and precipitation, under the influence of regional changes in groundwater depths (Brand et al., 1998). Also, relatively high Ni grades, which are enriched in garnierite minerals precipitated in the open fractures of this tend to be located beneath flat slope and slight slope areas (topographic categories V and IV) (Fig. 18A and B). The most likely reason for this is that slopes of topographic category IV were the most strongly fractured and, consequently, became the most deeply weathered. This is supported by the finding that the mean thickness of both the limonite and saprolite

reach their maximum in this topographic category (Fig. 6). Therefore, high Ni grade zones appear to be associated with the orientations of the paleo-groundwater flow, and this flow direction can be estimated by the statistical distribution of the thickness of laterization in which goethite is formed.

Ni transport and precipitation by the paleo-groundwater flow can be supported by correlations of Ni grades in the laterization layers. The Ni grades in the limonite, saprolite, and bedrock layers in a borehole were averaged in each layer and the averages between two layers were compared (Fig. 19). All three parts of two layers show absence of the correlation because the R^2 values are smaller than 0.1. This suggests that the Ni anomalies were not only originated from the nearby basement rocks but also the groundwater flow around the anomalies.

The highest Ni content (2.10% by XRF and 2.36% by EDX) was found in the saprolite layer in Zone 2 (Table 4) where dunite, containing more olivine than harzburgite, forms the basement. This suggests a local effect of the type of bedrock on the Ni grade.

Replacement of Mg or Fe by Ni can occur relatively easily because their atomic radii are similar (British Geological Survey, 2008) and Mg can enter solution and be transported by groundwater in a highly mobile fashion to significant depth in the deposit. As a result of this, and because Ni is relatively immobile, most Ni is concentrated at shallow depths, i.e. near surface and in the limonite layer. However, some Ni can be transported to greater depths along with Mg, by dissolution in groundwater. While Fe is insoluble in the groundwater, it reacts easily with oxygen to yield iron oxide that dissolves by hydration, as follows:



Accordingly, enrichment of hydrated iron oxide occurred near the Earth's surface or in the limonite layer. Goethite is the most typical

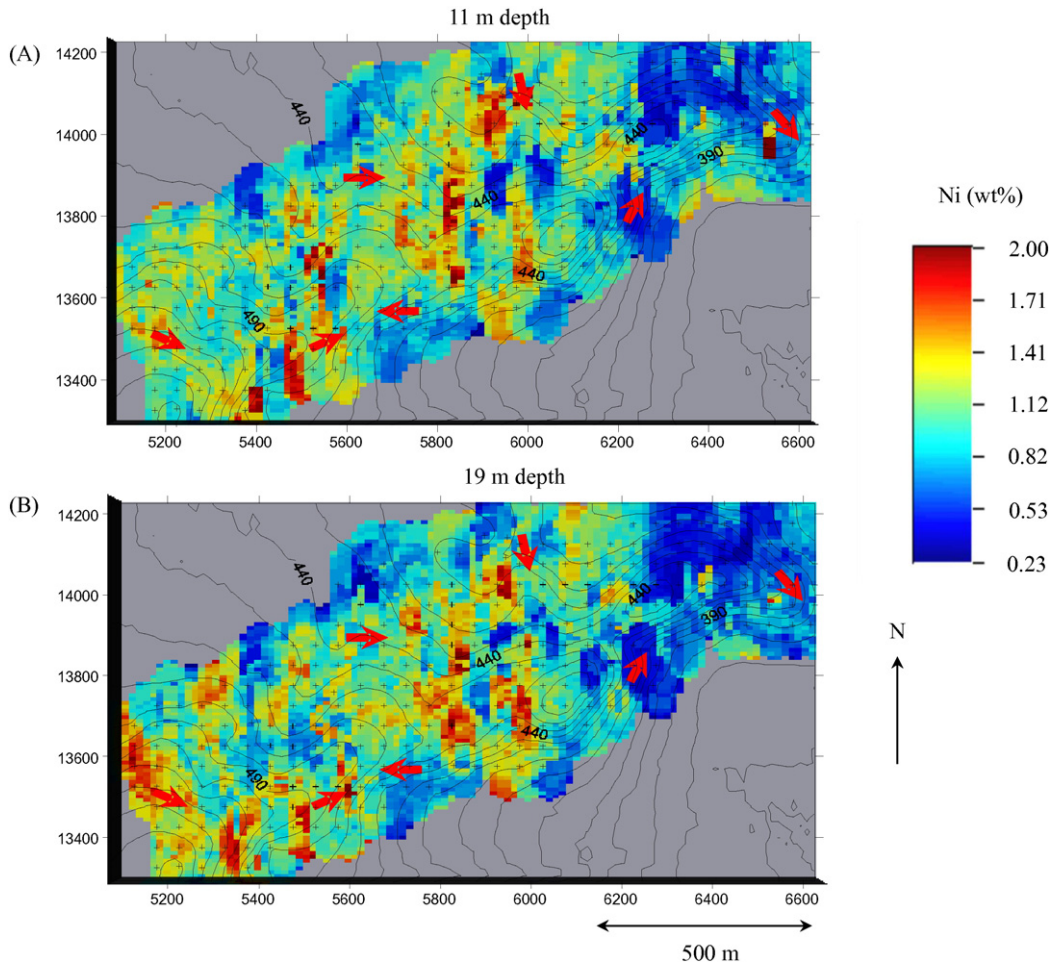
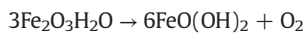


Fig. 16. Superimposition of the estimated paleo-groundwater flow directions (arrows) upon horizontal slices of the Ni grade distribution model in Fig. 9. A. Horizontal slice at 11 m depth. B. Horizontal slice at 19 m depth.

mineral generated from the weathering-based reduction of hydrated iron oxide, shown as follows:



Goethite has isostructural equivalents in which cations are occupied in interstices between oxygen frameworks. This structure suggests a possible occurrence of isomorphous substitution of Fe^{3+} , placed at the center of octahedral coordination, by the other cations such as Ni (Zeissink, 1969; de Oliveira et al., 1992; Alvarez et al., 2008). According to a bulk chemical analysis (Golightly and Arancibia, 1979), most irons in the weathered serpentines were found as ferric. Oxidation is the most typical weathering phenomenon related to groundwater and occurred effectively near the groundwater table. Therefore, iron compounds are easily oxidized and changed to ferric hydroxides such as goethite. Although the solubility of Ni compounds is small, they are soluble in acid groundwater with increasing temperature and decreasing pH (WHO, 2007) and then, Ni hydrates can migrate with groundwater. One possible origin of such acidity is decay of surface vegetation that can provide much CO_2 to infiltrated meteoric water. Groundwater flows from high (shallow) to low (deep) water table, which corresponds to migration of Ni hydrates from thin to thick laterized layer (sum of limonite and saprolite layers). With depth groundwater becomes progressively less acidic. Adsorption of Ni onto goethitic colloids might occur at neutral to slightly alkaline condition (Robb, 2005) that is possibly formed to be wider in the downstream of groundwater because of deepening of groundwater table and decrease in water velocity, and/or the above substitution of Fe^{3+} by Ni might occur at the condition. The

substitution is controlled by various properties such as size, electronegativity, and crystal field substitution energy of goethite crystal (Chavez et al., 2009). Thus, the presence of Ni accumulation in laterized layers can be used as an indicator of the presence of a groundwater system that carried Ni.

5. Conclusions

This study was aimed at determining the controlling factors of Ni grade distribution in 3D, in the high-grade zones of a Ni laterite deposit of central Sulawesi Island, Indonesia. The interpretation of borehole data from 294 sites, in conjunction with geostatistical analysis, has yielded the following main conclusions:

1. Spatial correlations of Ni data, as represented in semivariograms, were best approximated by a spherical model in both horizontal and vertical directions.
2. Ordinary kriging was used for the 3D modeling of Ni grade distribution because the correlation between Ni grade and other chemical components (Fe, SiO_2 , and MgO) was weak. High Ni grades were found to be generally concentrated in the saprolite layer under slight slope topography (category IV) with slope angles in the 5–19° range. Such slopes are characterized by the most strongly fractured geology because of their structure and/or the concentration of tectonic stress and consequently have become deeply weathered.
3. Goethite was identified in both the limonite and saprolite layers common to all seven zones studied. The presence of goethite in the laterized layers is considered an effective indicator of the presence

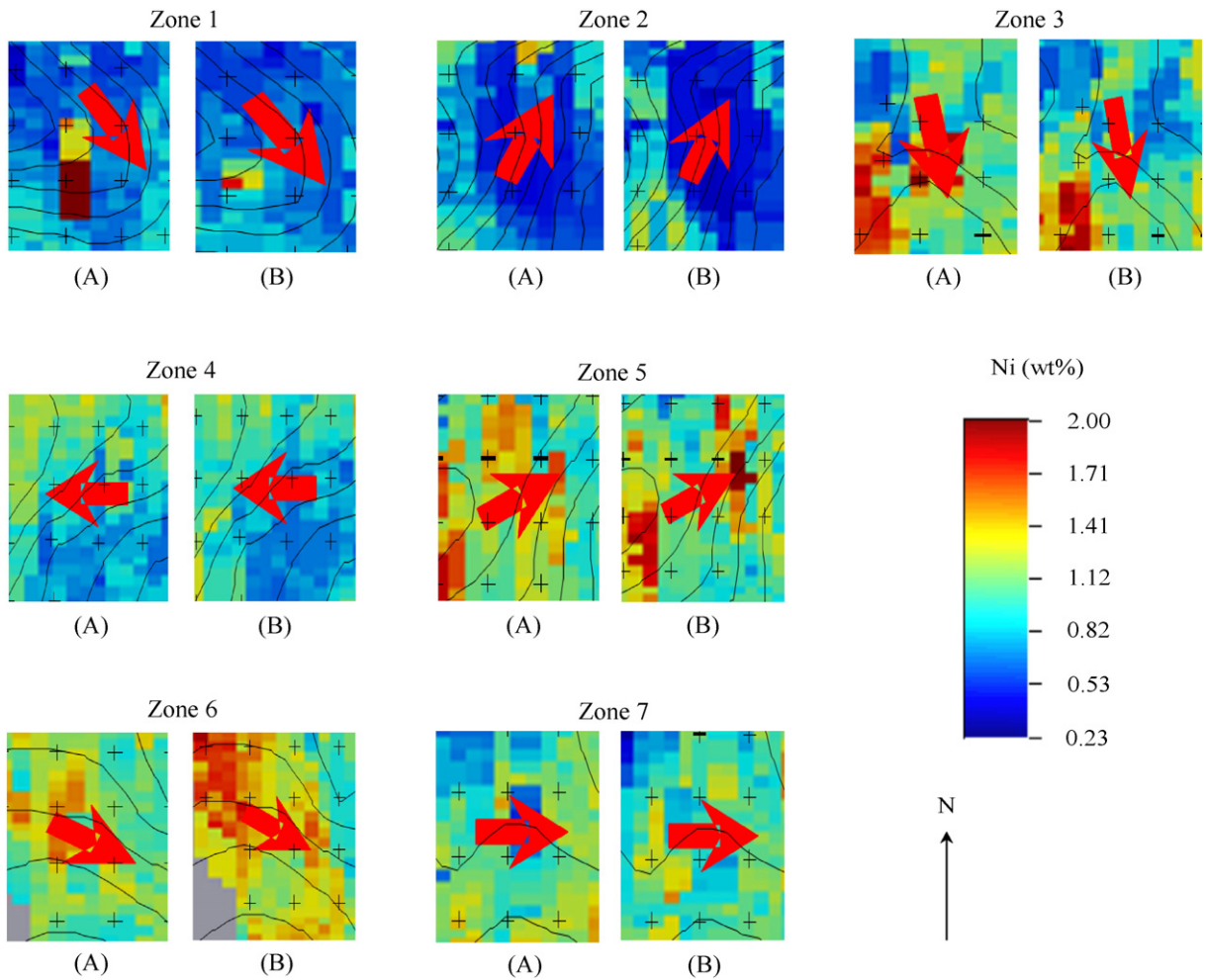


Fig. 17. Enlargements of the estimated paleo-groundwater flow directions and Ni grade distributions in the seven zones. Letters (A) and (B) for each zone denote 11 m and 19 m depth, respectively. The estimated flows tend to be directed from low to relatively higher Ni grades in each zone.

- of a paleo-groundwater system because of Fe replacement in goethite by Ni in the crystal lattice.
4. The vertical semivariograms of the Ni, Fe, SiO₂, and MgO contents in each of the seven zones were approximated in all cases by a spherical model, with the resultant ranges being similar. The thicknesses of the limonite layer were estimated by the average range because of the long-term weathering down to bedrock.
 5. Taking into account the thicknesses of the limonite and saprolite layers, and by superimposing the estimated flow directions upon the Ni grade distribution, it was possible to identify that the paleo-

groundwater flow directions were generally directed from lower to relatively higher Ni grades in all seven zones. This correspondence supports water–rock interaction being the primary mechanism of Ni dissolution and transport and precipitation by supergene processes that concentrated the Ni content as a result.

Acknowledgements

The authors express their sincere thanks to PT. INCO Indonesia for permission to use the data set. Sincere thanks are extended to Dr.

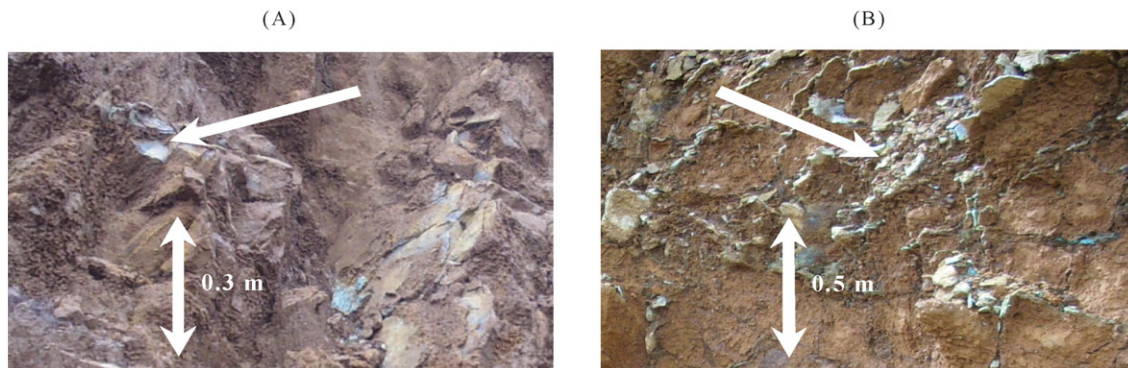


Fig. 18. Selected outcrops showing garnierite minerals with relatively high Ni grade (shown by arrows), which were precipitated in the open fractures around the Zone 7 located in the flat slope associated with a valley area or cavity (category V) (A) and around the Zone 3 located in the slight slope area (category IV) (B).

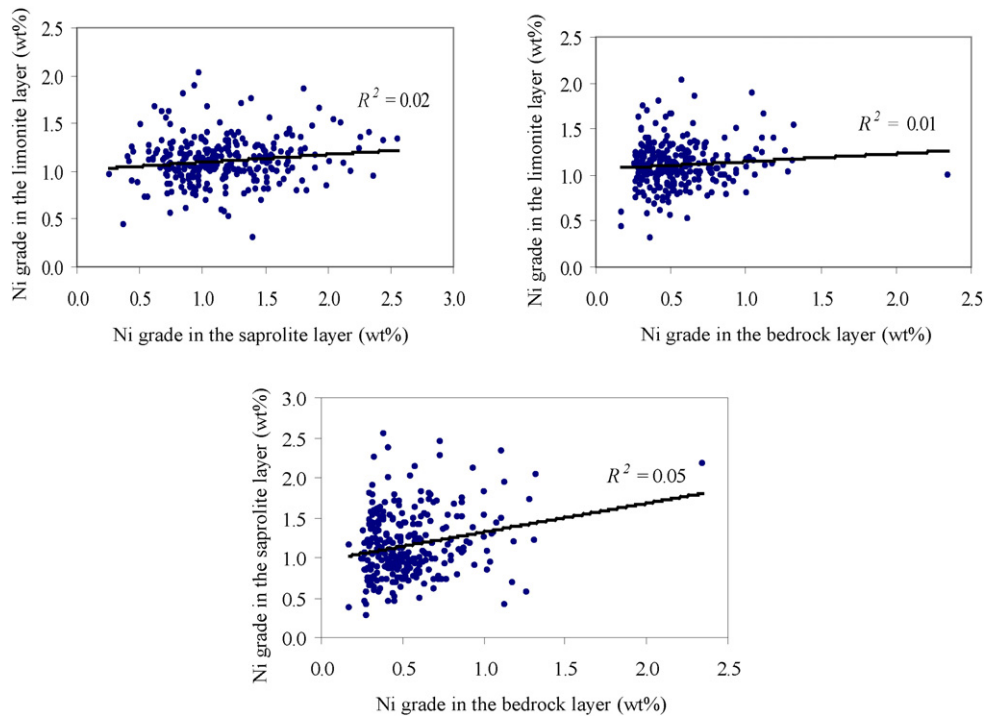


Fig. 19. Scattergrams for the relationship of Ni grade averages between two layers out of limonite, saprolite, and bedrock layers at each borehole. All pairs show absence of the correlation because of the R^2 values are smaller than 0.1.

Eishi Kusaka and Dr. Masakatsu Hasegawa of the Graduate School of Energy Science, Kyoto University for instruction in XRD analysis and to the GelK Program of Kumamoto University for supporting the field survey undertaken by the first author. The authors would like also to express their sincere thanks to the anonymous reviewers and the editor for the valuable, constructive, and preferable comments. This work was partially supported by JSPS KAKENHI grant number 26120519.

References

- Alevizos, G., Repouskou, E., 2011. Ore microscopy and microanalysis of the nickeliferous iron ores from Komnina Vermion area (N. W. Greece). *Geomaterials* 1, 46–50.
- Alvarez, M., Sileo, E.E., Rueda, E.H., 2008. Structure and reactivity of synthetic Co-substituted goethites. *Am. Mineral.* 93, 584–590.
- Brand, N.W., Butt, C.R.M., Elias, M., 1998. Nickel laterites: classification and features. *AGSO J. Aust. Geol. Geophys.* 17 (4), 81–88.
- Briggs, I.C., 1974. Machine contouring using minimum curvature. *Geophysics* 39 (1), 39–48.
- British Geological Survey, 2008. Nickel. *Industry News*, pp. 1–24. Keyworth, Nottingham, United Kingdom. (Url: <https://www.bgs.ac.uk/mineralsuk/industry/2008/08nov.html#nickel>).
- Chavez, L.H.G., Curry, J.E., Stone, D.A., Carducci, M.D., Chorover, J., 2009. Nickel incorporation in Fe(II, III) hydroxysulfate green rust: effect on crystal lattice spacing and oxidation products. *Rev. Bras. Ciênc. Solo* 33, 1115–1123.
- Cluzel, D., Vigier, B., 2008. Syntectonic mobility of supergene nickel ores of New Caledonia (Southwest Pacific), evidence from garnierite veins and FAULTED regolith. *Resour. Geol.* 58 (2), 161–170.
- Colin, F., Nahon, D., Trescases, J.J., Melfi, A.J., 1990. Lateritic weathering of pyroxenites at Niquelandia, Goiaz, Brazil: the supergene behavior of nickel. *Econ. Geol.* 85, 1010–1023.
- Dalvi, A.D., Bacon, W.G., Osborne, R.C., 2004. The past and the future of nickel laterites. *Inco Limited, Ontario, Canada*, pp. 1–27.
- de Oliveira, S.M.B., Trescases, J.J., Melfi, A.J., 1992. Lateritic nickel deposits of Brazil. *Mineral. Deposita* 27, 137–146.
- de Vletter, D.R., 1978. Criteria and problems in estimating global lateritic nickel resources. *Math. Geol.* 10 (5), 533–542.
- Dowd, P.A., 1992. Geostatistical ore reserves estimation: a case study in a disseminated nickel deposit. *Geol. Soc. Lond. Spec. Publ.* 63, 243–255.
- Emery, X., 2006. Two ordinary kriging approaches to predicting block grade distributions. *Math. Geol.* 38 (7), 801–819.
- Evans, A.M., 1987. *An introduction to ore geology*. second ed. Blackwell Scientific Publications, Oxford, pp. 268–279.
- Gallardo, T., Tauler, E., Proenza, J.A., Lewis, J.F., Gali, S., Labrador, M., Longo, F., Bloise, G., 2010. Geology, mineralogy and geochemistry of the Loma Ortega Ni laterite deposit, Dominican Republic. *Macla* 13, 89–90.
- Gleeson, S.A., Butt, C.R.M., Elias, M., 2003. Nickel laterites: a review. *Society of Economic Geologists Newsletter*. 54, pp. 9–16.
- Golightly, J.P., 1979. *Geology of Soroako nickeliferous laterite deposit*. INCO Metals Company, Ontario, Canada.
- Golightly, J.P., Arancibia, O.N., 1979. The chemical composition and infrared spectrum of nickel- and iron-substituted serpentine from a nickeliferous laterite profile, Soroako, Indonesia. *Can. Mineral.* 17, 719–728.
- Guilbert, J.M., Park Jr., C.F., 1986. *The geology of ore deposits*. W. H. Freeman and Company, New York, pp. 774–789.
- Herrington, R., Boni, M., Skarpelis, N., Large, D., 2007. Paleoclimate, Weathering And Ore Deposits – A European Perspective. *Proceedings of the Ninth Biennial SGA Meeting*, pp. 1373–1376.
- Ilyas, A., Koike, K., 2012. Geostatistical modeling of ore grade distribution from geomorphic characterization in a laterite nickel deposit. *Nat. Resour. Res.* 21 (2), 177–191.
- Kadarusman, A., Miyashita, S., Maruyama, S., Parkinson, C.D., Ishikawa, A., 2004. Petrology, geochemistry and paleogeographic reconstruction of the East Sulawesi Ophiolite, Indonesia. *Tectonophysics* 392, 55–83.
- Koike, K., Gu, B., Ohmi, M., 1998. Three-dimensional distribution analysis of phosphorus content of limestone through a combination of geostatistics and artificial neural network. *Nonrenewable Resour.* 7 (3), 197–210.
- Kubo, K., 2001. Dunitic formation processes in highly depleted peridotite. Case study of the Iwanadake peridotite, Hokkaido, Japan. *J. Petrol.* 43 (3), 423–448.
- Lewis, J.F., Draper, G., Proenza, J.A., Espaillet, J., Jimenez, J., 2006. Ophiolite-related ultramafic rocks (serpentinites) in the Caribbean Region: a review of their occurrence, composition, origin, emplacement and Ni laterite soil formation. *Geol. Acta* 4 (1-2), 237–263.
- Macpherson, C.G., Hall, R., 2002. Timing and tectonic controls in the evolving orogen of SE Asia and the Western Pacific and some implications for ore generation. *Geol. Soc. Lond. Spec. Publ.* 1–19.
- Mitasova, H., Mitas, L., 1993. Interpolation by regularized spline with tension: I. Theory and Implementation. *Math. Geol.* 25 (6), 641–655.
- Mubrotto, B., Briden, J.C., McClelland, E., Hall, R., 1994. Paleomagnetism of the Balantak ophiolite, Sulawesi. *Earth Planet. Sci. Lett.* 125, 193–209.
- Pelletier, B., 1996. Serpentinites in nickel silicate ores from New Caledonia. *Publication Series* 6(9). Australasian Institute of Mining and Metallurgy, Melbourne, pp. 197–205.
- Proenza, J.A., Lewis, J.F., Gali, S., Tauler, E., Labrador, M., Melgarejo, J.C., Longo, F., Bloise, G., 2008. Garnierite mineralization from Falcondo Ni-laterite deposit (Dominican Republic). *Macla* 9, 197–198.
- PT. INCO Indonesia., 2006. Inventory of mineral resources and mineral reserves. Unpublished report (in Bahasa Indonesia).
- Robb, L., 2005. *Introduction to ore-forming processes*. Blackwell Science Ltd., USA, pp. 219–229.
- Sadeghi, B., Madani, N., Carranza, E.J.M., 2015. Combination of geostatistical simulation and fractal modeling for mineral resource classification. *J. Geochem. Explor.* 149, 59–73.
- Sagapoa, C.V., Imai, A., Watanabe, K., 2011. Laterization process of ultramafic rocks in Siruka, Solomon Islands. *Novel Carbon Resour. Sci.* 3, 32–39.
- Soler, J.M., Cama, J., Gali, S., Melendez, W., Ramirez, A., Estanga, J., 2008. Composition and dissolution kinetics of garnierite from the Loma de Hierro Ni-laterite deposit, Venezuela. *Chem. Geol.* 249, 191–202.

- Srivastava, R.M., 2005. Probabilistic modeling of ore lens geometry: an alternative to deterministic wireframes. *Math. Geol.* 37 (5), 513–544.
- Suratman, 2000. Geology of laterite nickel deposit in Sorowako area, South Sulawesi Province. Proceedings of 29th Indonesian association of geologists, Bandung, Indonesia, pp. 37–43.
- Talovina, I.V., Lazarenkov, V.G., Ryzhkova, S.O., Ugol'kov, V.L., Vorontsova, N.I., 2008. Garnierite in nickel deposits of the Urals. *Lithol. Miner. Resour.* 43 (6), 588–595.
- Thorne, R., Herrington, R., Roberts, S., 2009. Composition and origin of the Caldag oxide nickel laterite, W. Turkey. *Mineral. Deposita* 44, 581–595.
- Thorne, R.L., Roberts, S., Herrington, R., 2012. Climate change and the formation of nickel laterite deposits. *Geology* 40, 331–334.
- Van Zuidam, R.A., 1985. Terrain analysis and classification using aerial photographs. ITC-Textbook, second ed. International Institute for Aerial Survey and Earth Sciences, Enschede, Netherland (VII-6).
- Verly, G., 2005. Grade control classification of ore and waste, a critical review of estimation and simulation based procedures. *Math. Geol.* 37 (5), 451–475.
- WHO, 2007. Nickel in drinking water. WHO/SDE/WSH/07.08/55. World Health Organization, Geneva.
- Zeissink, H.E., 1969. The mineralogy and geochemistry of a nickeliforous laterite profile (Greenvale, Queensland, Australia). *Mineral. Deposita* 4, 132–152.